


Article

Influence of Laser Additive Manufacturing and Laser Polishing on Microstructures and Mechanical Properties of High-Strength Maraging Steel Metal Materials

Haibing Xiao ¹ , Yongzhang Chen ^{1,2}, Mingjun Liu ^{1,*}, Yongquan Zhou ¹, Chenlin Du ² and Wei Zhang ¹

¹ Intelligent Manufacturing and Equipment School, Shenzhen Institute of Information Technology, Shenzhen 518172, China

² Key Laboratory of Advanced Optical Precision Manufacturing Technology of Guangdong Higher Education Institutes, Shenzhen Technology University, Shenzhen 518060, China

* Correspondence: liumj@szit.edu.cn; Tel.: +86-755-8922-6591

Abstract: To increase the surface quality of the high-strength maraging steel metal materials, a new method of executing the additive manufacturing process and subtraction polishing process of maraging steel metal materials was studied. The mechanical properties of maraging steel metal materials before and after laser powder bed fusion (LPBF) polishing were compared and analyzed. The influence of laser parameters on the formability of high-strength MS metal materials was studied, with MS additive parts successfully prepared. The initial surfaces had roughness values of 6.198–7.92 μm . The metal additive manufacturing parts were polished with double laser beams. Confocal microscopy, scanning electron microscopy, and X-ray diffraction were used to obtain the microstructure and phase composition of the microstructures. The microhardness of high-strength maraging forming parts by using a microhardness tester and the mechanical properties were analyzed. The results showed that the surface roughness was considerably reduced to lengthen the service life of the high-strength MS metal materials from an initial roughness of $S_a = 6.3 \mu\text{m}$ to $S_a = 0.98 \mu\text{m}$, with the surface hardness increased and the martensite content decreased after using double-laser-beam polishing.

Keywords: metal additive manufacturing; high-strength maraging steel metal material; structure design; topology optimization; double-laser-beam polishing



Citation: Xiao, H.; Chen, Y.; Liu, M.; Zhou, Y.; Du, C.; Zhang, W. Influence of Laser Additive Manufacturing and Laser Polishing on Microstructures and Mechanical Properties of High-Strength Maraging Steel Metal Materials. *Appl. Sci.* **2022**, *12*, 10340. <https://doi.org/10.3390/app122010340>

Academic Editors: Changjun Han and Changhui Song

Received: 29 August 2022

Accepted: 8 October 2022

Published: 14 October 2022

Publisher's Note: MDPI stays neutral with regard to jurisdictional claims in published maps and institutional affiliations.



Copyright: © 2022 by the authors. Licensee MDPI, Basel, Switzerland. This article is an open access article distributed under the terms and conditions of the Creative Commons Attribution (CC BY) license (<https://creativecommons.org/licenses/by/4.0/>).

1. Introduction

Metal laser additive manufacturing (AM), commonly known as metal 3D printing, combines design, laser material processing, and forming technology. It is based on digital model files and uses software and numerical control systems to construct specialized metal materials layer by layer via extrusion, sintering, melting, light curing, and spraying. Metal additive manufacturing has the advantages of being highly integrated, having a complex geometric design, and saving time in the aerospace, machine building, automotive, and energy industries [1–4]. In contrast with other conventional subtractive manufacturing or formative manufacturing processes, AM is a process in which the feedstocks are stacked layer by layer based on 3D trajectory data [5–7]. Metal 3D printing has become the focus of researchers because of its considerable advantages in processing high-strength steel materials such as rapid prototyping, the possibility of adjusting phase structure, flexibility, and extending possible uses of high-strength steel materials [8–10]. Though metal 3D printing has been extensively studied and substantial progress has been made in material flexibility and mechanical performances, many defects still exist in the fabricated parts. These defects, including porosity, cracking, laser spatter, shape distortion, open pores on the surface, and poor surface finish, affect the performance of the parts and limited their scope of application [11,12]. In recent years, several research groups have aimed to investigate the factors that lead to the poor surface quality of the parts fabricated by AM and have

made efforts to enhance their performance. Laser polishing, electrochemical polishing, abrasive flow machining, and chemical polishing are commonly used to reduce surface roughness [13–16]. Compared with conventional abrasive or chemical techniques, laser polishing based on melting materials has the advantages of being a non-contact process, highly repeatable, environmentally friendly, and having low labor costs and a convenient operation [17]. Furthermore, the AM process using laser technology allows for the in situ polishing of the initially formed parts using the same machine [18]. In 2013, Strano et al. [19] studied the surface roughness and topography of 316L steel alloy parts made with selective laser melting. The results demonstrated that the particles that stuck along the step edges affected the surface roughness by filling in the gaps between the consecutive layers. A previous study [20–22] summarized recent findings on the quality of LPBF parts from maraging steel and other materials. Some studies [23,24] involving the tune of multi-material additive manufacturing laser powder bed fusion (LPBF) manufactured have been conducted. Mower et al. [25] systematically studied the mechanical behavior of metallic alloys fabricated using different AM and other methods.

Some authors have investigated laser polishing SLM surfaces, but mostly for titanium alloys, with some for 316L thin section parts [26], SLM fabricated Ti-6Al-4V components [27], or additive-manufactured Ti-based alloys [28]. To our best knowledge, laser polishing has been explored by many authors, including a recent study by Yung et al. [29], who have been developing a new polishing method in order to polish the additive manufactured CoCr alloy components with complex surface shape. The resulting surface roughness was reduced by up to 93% and the mechanical hardness of the laser-polished samples was enhanced by 8%. Li et al. [30] demonstrated that the performance of Ti alloys prepared by LPBF could be observably enhanced via a laser polishing technique, with the surface roughness effectively reduced from 6.53 to 0.32 μm . In 2021, Bhaduri et al. [31] proposed a novel laser polishing strategy to reduce the average roughness of aluminum alloy parts. When processing with a nanosecond-pulsed laser, a sub-micron surface roughness was achieved. Parvez et al. [32] proposed a novel laser-aided machining and polishing process approach to remarkably increase the surface quality of deposited parts.. Rosa et al. [33,34] studied the methods and techniques for laser polishing additive laser manufacturing surfaces. Yao [35] studied the process optimization concept of combining additive manufacturing and surface polishing processes. Temmler et al. [36], from Tsinghua University, the Fraunhofer Institute, and RWTH Aachen University, studied the effect of laser polishing on the surface roughness and properties of the remelting surface of H11 tool steel. Willenborg [37], a world-famous laser polishing expert, proposed a new method including a top-hat scanning strategy for the laser polishing of additively manufactured polymer parts. Experiments on laser processing polishing of LPBF maraging steel were conducted to increase the quality of LPBF maraging steel [38].

In previous research, laser metal additive for high-strength steel materials has been studied. There is an expected impact on fatigue and fracture strength of these materials, as cracks generally initiate at steel's surface irregularities [39,40]. The methods researchers use to improve the surface mechanical properties and reduce the surface roughness of metal additive manufacturing parts is a key aspect needing to be considered in laser manufacturing technology. At present, the laser polishing metal additive manufacturing of high-strength maraging steel metal material can be used to create high-strength metal parts, generally reducing their roughness to 2–3 μm . In this work, we established a new process for the additive and subtractive metal manufacturing of high-strength steel using double-laser-beam polishing. The influence of laser additive manufacturing and laser polishing on the microstructures and mechanical properties of high-strength MS metal materials are revealed.

2. Principle of Additive and Subtractive Manufacturing of High-Strength Metal Materials

Laser power bed fusion (LPBF) uses laser irradiation on pre-laid metal powder. Specifically, after forming metal parts, the lasers are completely covered with powder and a

finely focused light spot is used to quickly melt the preset powder, meaning that functional parts based on the metallurgical combination of almost any shape can be obtained. For these, the density can reach 100%, the dimensional accuracy can reach 20–50 μm , and the surface roughness can reach 20–30 μm . The metal laser additive manufacturing process of high-strength metal materials based on selective melting is shown in Figure 1 [11,35].

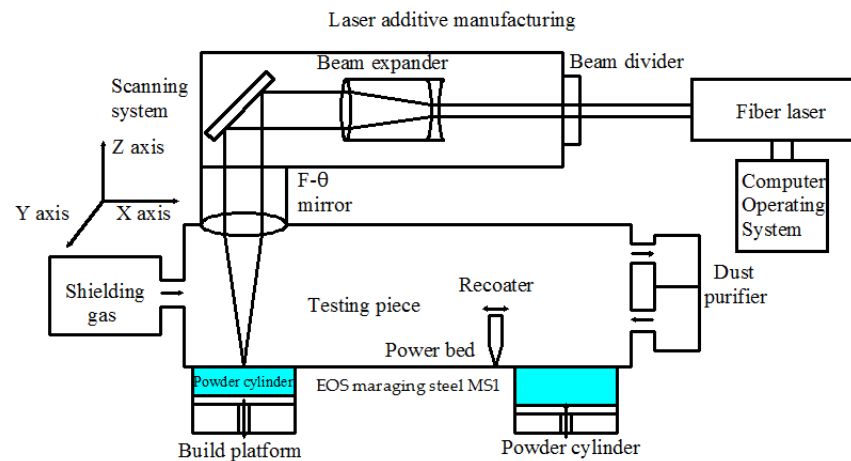


Figure 1. Metal additive manufacturing of high-strength metal material based on selective melting.

The surface of the metal additive manufacturing samples is rough and they are difficult to directly use; thus, we propose the use of a double-laser-beam polishing method for microsubtraction manufacturing. The dual-beam laser polishing method for metal additive manufacturing parts is shown in Figure 2. The illustration reveals the overall scheme for polishing high-strength steel equipment with dual-laser beams.

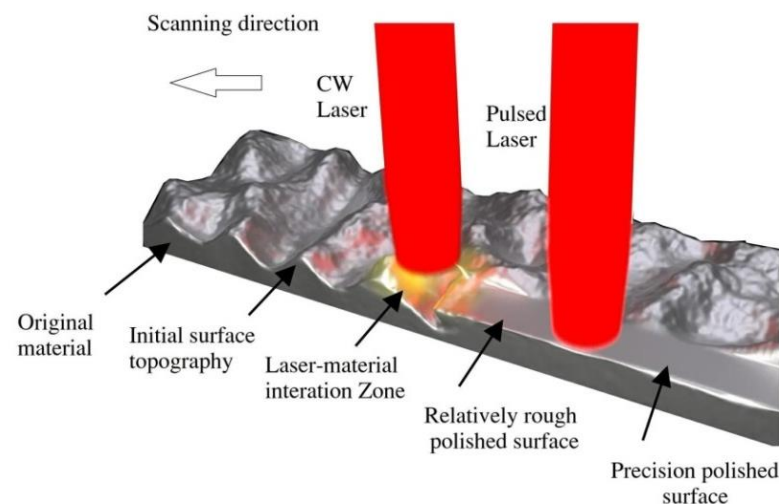


Figure 2. Method of dual-beam laser polishing metal additive manufacturing parts.

Taking a polishing cavity as an example, its working principle is as follows: Under the protection of an inert gas sealing chamber, a continuous laser (power 300–800 W, top-hat flat-top beam) acts on the special-shaped surface of metal additive manufacturing samples through the front-focusing three-dimensional galvanometer to achieve the purpose of preheating and rough polishing. A pulsed laser, appearing through a front-focusing 3D vibrator, then rapidly melts the microsurface crest of the irregular curved surface in a small local area with an appropriate pulse peak energy and fills in the troughs (commonly known as the “melting peak filling valleys”), thus reducing the surface roughness. The existing laser polishing technique uses the melting peak filling valleys technology principle

to achieve a flat surface, and this is called micro material reduction manufacturing. In the double-laser-beam technique, a high-power continuous laser is first used for rough polishing, followed by a low-power pulse laser for fine polishing. We used composite path double-laser-beam polishing and double-laser-beam composite path scanning, so that the molten pool was uniformly distributed and to reduce the molten pool temperature gradient. The energy required by a continuous laser, to achieve turbulent metal and to achieve a complete “peak”, is larger; therefore, an overflow phenomenon will occur in the molten pool (reported in [41]). There are many process factors in dual-beam laser polishing.

3. Materials and Methods

3.1. EOS M290 Metal Additive Manufacturing

The EOS M290 laser metal additive manufacturing system used was equipped with a 400W fiber laser to provide a high-performance laser light source. The EOS M290 LPBF system is shown in Figure 3a; it consists of a new modules EOS powder bed, an EOSTATE base, and an EOSTATE laser monitoring to meet industry needs and improve quality management. Figure 3b depicts flow diagrams showing the LPBF processes. The EOS M290 metal additive manufacturing system, which has been updated three times, is installed in the forming chamber to detect the powdering of each layer and to take pictures. The EOSTATE base provides real-time monitoring of the Z-axis position, laser power, scanning accuracy, forming chamber temperature, forming chamber humidity, pressure, and other parameters. EOS laser monitoring is a laser monitoring module that monitors the laser power in real time throughout the entire production process. It is equipped with a nitrogen generating and nitrogen and argon automatic switching device, gas protection system, gas advection dust recovery system, gas filtration system, automatic induction protective gas filtration system, and temperature detection system in the warehouse, with full-width active scanning detection, depowder system, and liquid vacuum depowder system.

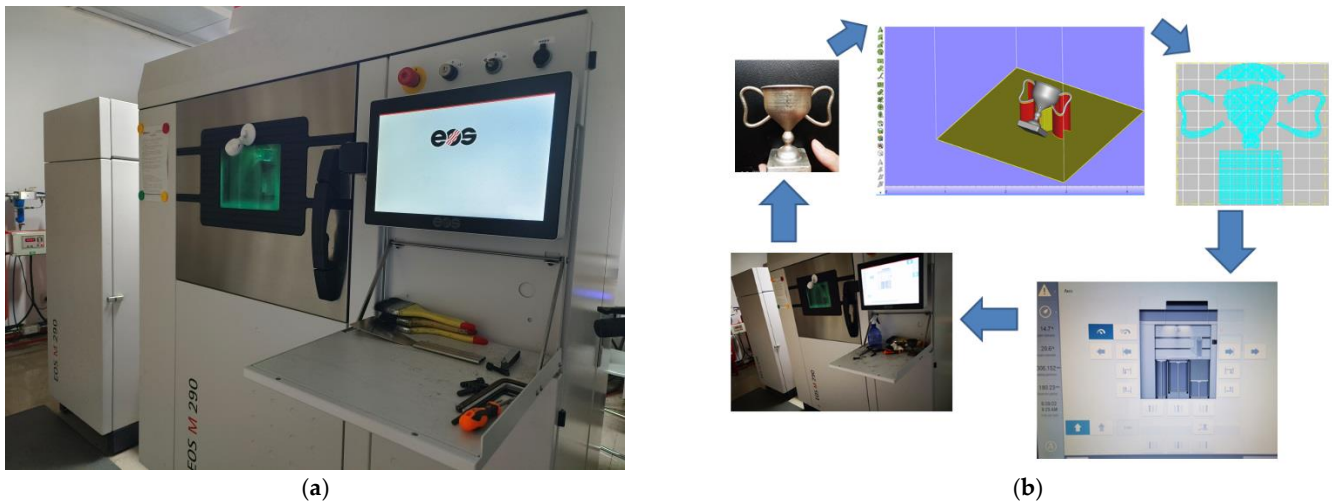
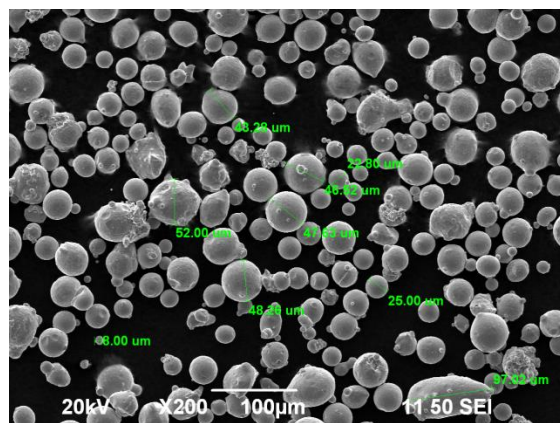


Figure 3. (a) Photograph of the EOS M290 LPBF system and (b) flow diagram showing the LPBF processes.

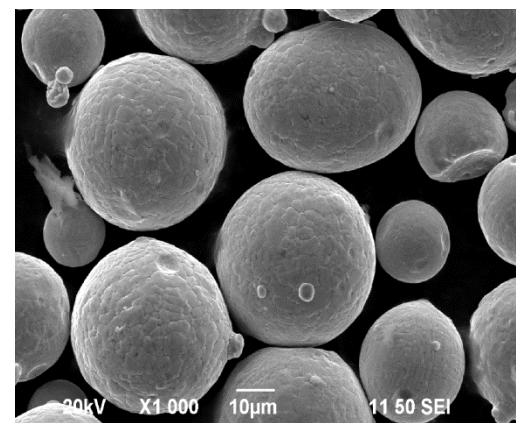
The parameters of the EOS M290 metal additive manufacturing system are shown in Table 1. EOS maraging steel MS1 is suitable for injection mold and engineering parts. SEM morphology of EOS maraging steel MS1 is shown in Figure 4. Figure 4a is the SEM photo magnified 100 times and Figure 4b is the SEM photo magnified 1000 times. The powder particles morphology was investigated in a prior study [19], while the chemical composition and weight (wt.%) of EOS maraging steel MS1 is shown in Table 2 [42].

Table 1. Parameters of the EOS M290 metal additive manufacturing system.

Parameters of the Category	Numerical Value	Parameters of the Category	Numerical Value
Maximum molding size	250 mm × 250 mm × 325 mm	Optical scanning system	F-theta
Type of laser	Yb-fiber	Scanning speed	Highest 7.0 m/s
Laser power	400 W	Power	Maximum 8.5 kW
3D printing speed	5–20 cm ³ /h	Thickness	20–100 µm
Laser spot diameter	100–500 µm	Overall dimensions	2500 × 1300 × 2190 mm
Scanning system	SCANLAB galvanometer scanning system	Spread direction of powder	Horizontal, one-way powder
XY-axes laser accuracy	≤±6 µm	Z-axis powder accuracy	≤±10 µm



(a)



(b)

Figure 4. SEM morphology of EOS maraging steel MS1: (a) 100×, (b) 1000×.**Table 2.** Chemical composition and weight (wt.%) of EOS maraging steel MS1 [42].

Fe	Ni	Co	Mo	Ti	C	Al	Ti
67.552	17.59	9.2	4.86	0.64	0.05	0.079	0.64

3.2. Parameters of Dual-Beam Laser Polishing

Based on the preliminary research of our team [43], a dual-laser-beam five-axis polishing test platform (Figure 5) consisting of a dual-laser 3D galvanometer and a two-axis CNC rotary table was used. Using the polishing of the MS additive manufacturing part shown in Figure 1 as an example, the infrared continuous laser and pulsed laser with top-hat characteristics entered the 3D galvanometer of their respective front-focusing system. The movement of the focused laser spot on the surface of the three-dimensional cavity of the mold can be controlled by the Z-axis moving lens and the X-axis and Y-axis rotating lens. On the two axes, the rotation of the NC rotary table and mold cavity laser processing blind area, in the range of the 3D vibrating mirror machining, can be exposed. In this way, the galvanometer of the three movements in the X, Y, Z, and NC rotary table two axes linkage can be used to realize laser spot scanning in the mold cavity arbitrary area of the polishing processing. Parameters of the dual-beam laser polishing are shown in Table 3.

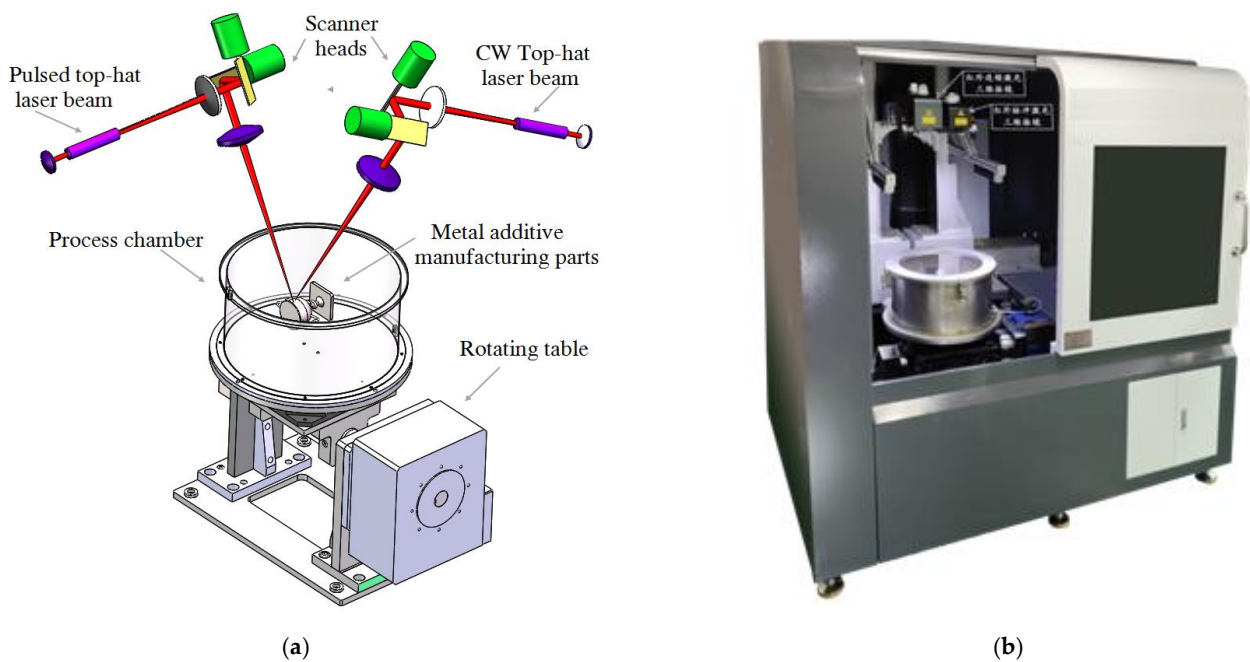


Figure 5. Dual-beam laser polishing system: (a) schematic diagram of the EOS M290 LPBF system, (b) photograph of dual-beam laser polishing system.

Table 3. Parameters of the dual-beam laser polishing.

Set-Up Laser Parameters	CW Laser	Pulsed Laser
Power	600 W	80 W
Wavelength	1080 nm	1064 nm
Pulse duration	N/A	1.3 μ s
Spot diameter	0.47 mm	0.32 mm
Scanning speed	800 mm/s	2000 mm/s
Step-over	0.1 mm	0.1 mm
Scanning route	zigzag	Zigzag-square wave

3.3. Methods for Microstructures and Mechanical Properties

A continuous laser and pulsed laser were used for multi-step polishing, remarkably reducing the surface roughness [27,43]. The filter values (S and L filter) from the roughness measurements are used to test roughness. The filtering parameters used for the surface analysis are Gaussian (ISO 16610-61). X-ray diffraction technology is used for before and after polishing surface characterization. The polishing layer was characterized by the roughness measurement tool (Mahr MarSurf CM mobile and Bruker), XRD (AD8 Advance), SEM (Zeiss Gemini SEM 300), and nano hardness tester (TI 950 Triboindenter). For quantitative XRD analysis, with 20 wt.% as the internal standard, the measurements were performed by D8 Advance X-ray diffractometer from Bruker Corp., at 40 mA and 40 KV with an angular scan of 5–65°.

4. Experiment and Analysis

4.1. Parameters of Dual-Beam Laser Polishing

The EOS M290 laser metal additive manufacturing system is a direct metal sintering system for the mass production of molds, metal parts, and fast-forming parts. The DMLS direct metal sintering system uses a laser beam to sinter ultrafine metal powder in layers, enabling complex designs such as complex surfaces, bending deep grooves, and three-dimensional channel designs to be realized. Except for the scanning speed, the surface

metal additive manufacturing method is similar to that used in previous works [44,45], with the MS1 metal additive manufacturing parameters optimized and shown in Table 4.

Table 4. MS1 laser additive process parameters and metal laser additive process parameters.

Laser Power (W)	Scanning Speed (mm/s)	Scanning Interval (mm)	Powder Thickness (μm)	Energy Density (J/mm^3)
300	750	0.12	55	69.4

The optimized process parameters of powder laser additive manufacturing were as follows: laser power, 300 W; laser scanning speed, 720 mm/s; pulse width, 2.0 ms to 4.0 ms; and scanning interval, 0.1 mm. Three sample parts formed by LPBF and which underwent high-strength additive manufacturing are shown in Figure 6. Figure 6a shows the high-strength steel additive manufacturing plane parts, Figure 6b shows the high-strength steel additive manufacturing small amplitude curved part, and Figure 6c shows the three-dimensional sample with large curvature. As can be seen from Figure 6, under this combination of optimized process parameters, the formed parts by laser additive manufacturing had essentially smooth surfaces and a high formability. Area A', B', C' are scale representative of Parts A, B and C respectively, representing different molding angles.

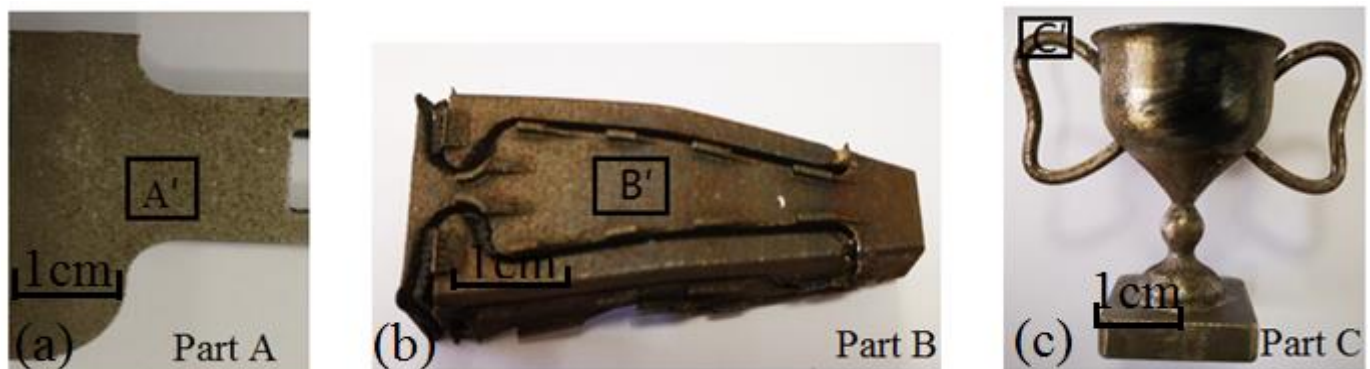
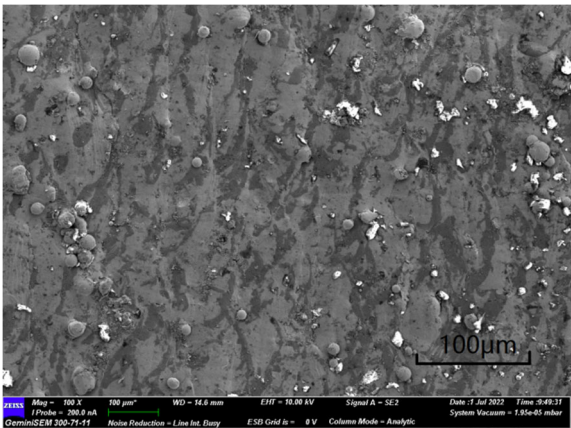
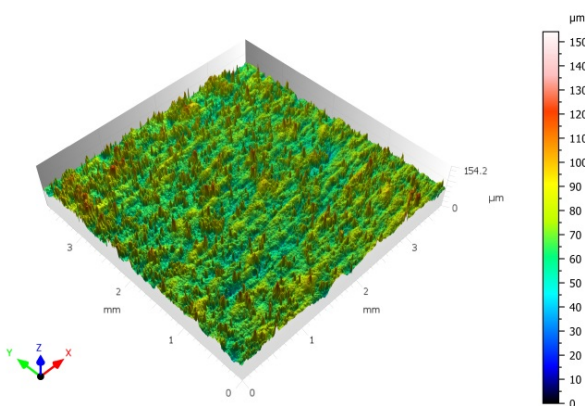


Figure 6. Three samples of high-intensity MS laser additive manufacturing. (a) High-strength steel additive manufacturing plane in Part A, (b) high-strength steel additive manufacturing small amplitude curved in Part B, and (c) three-dimensional sample with large curvature in Part C.

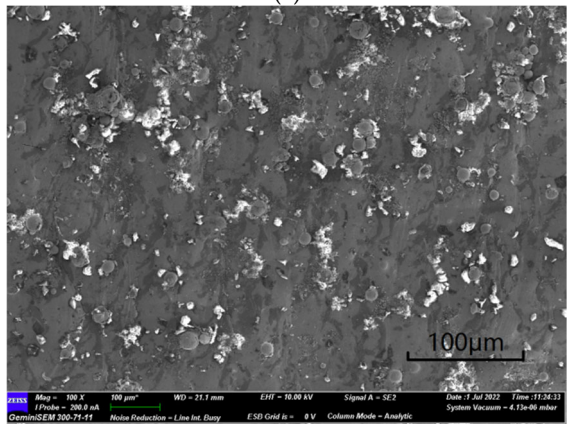
Figures 7–9 show the SEM images and 3D profiles of Parts A', Part B', and Part C'. The microstructures of the formed parts were dense, without macroscopic cracks and cavities, and their cell structures were at the submicron level, as can be seen from images taken by a high-power microscope. The additive manufacturing process parameters, properties of the materials, and geometry and shape of the parts all affected their surface morphology after forming. The initial Part A' surfaces had roughness values of 6.198 μm to 6.635 μm , the initial Part B' surfaces had roughness values of 6.888 μm to 6.922 μm , and the initial Part C' surfaces had roughness values of 7.128 μm to 7.92 μm . Therefore, it can be seen that with different forming structures and angles, the surface roughness is different.



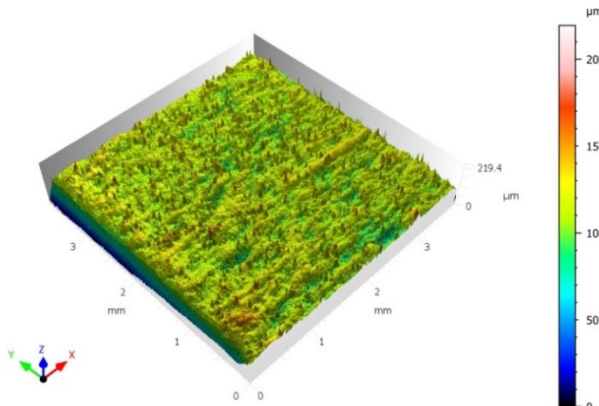
(a)



(b)

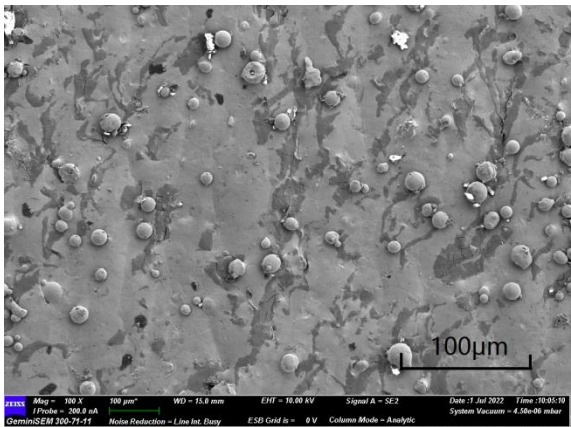


(c)

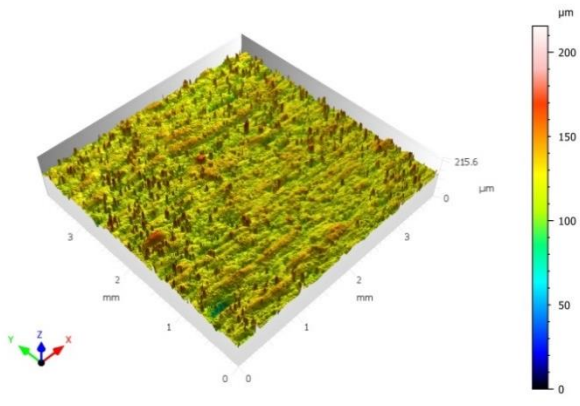


(d)

Figure 7. SEM images and 3D profiles of Part A': (a,b) horizontal plane; (c,d) vertical surface.



(a)



(b)

Figure 8. Cont.

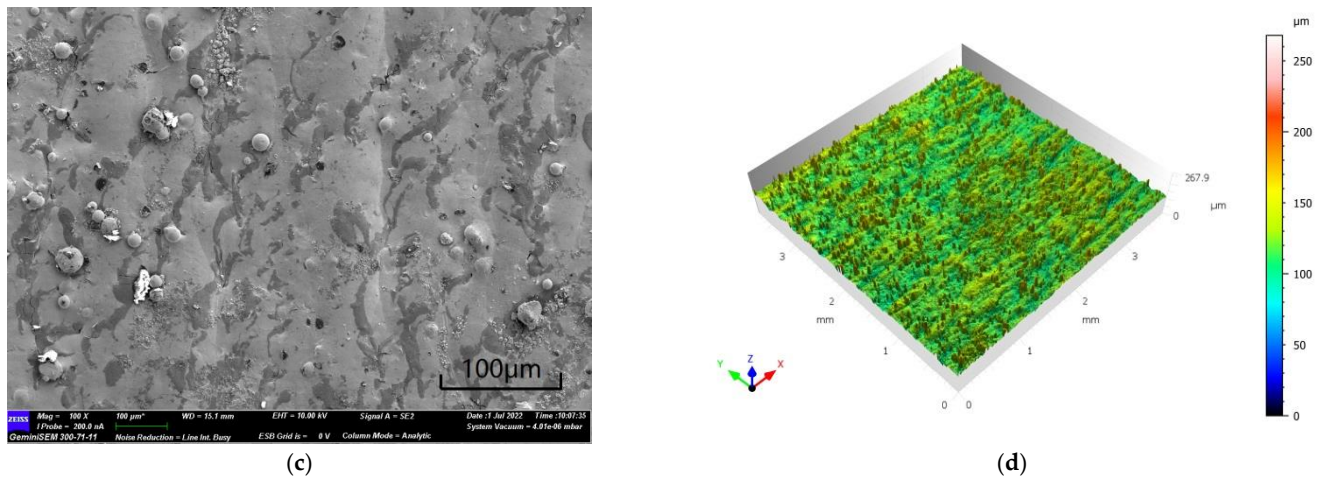


Figure 8. SEM images and 3D profiles of Part B': (a,b) horizontal plane; (c,d) vertical surface.

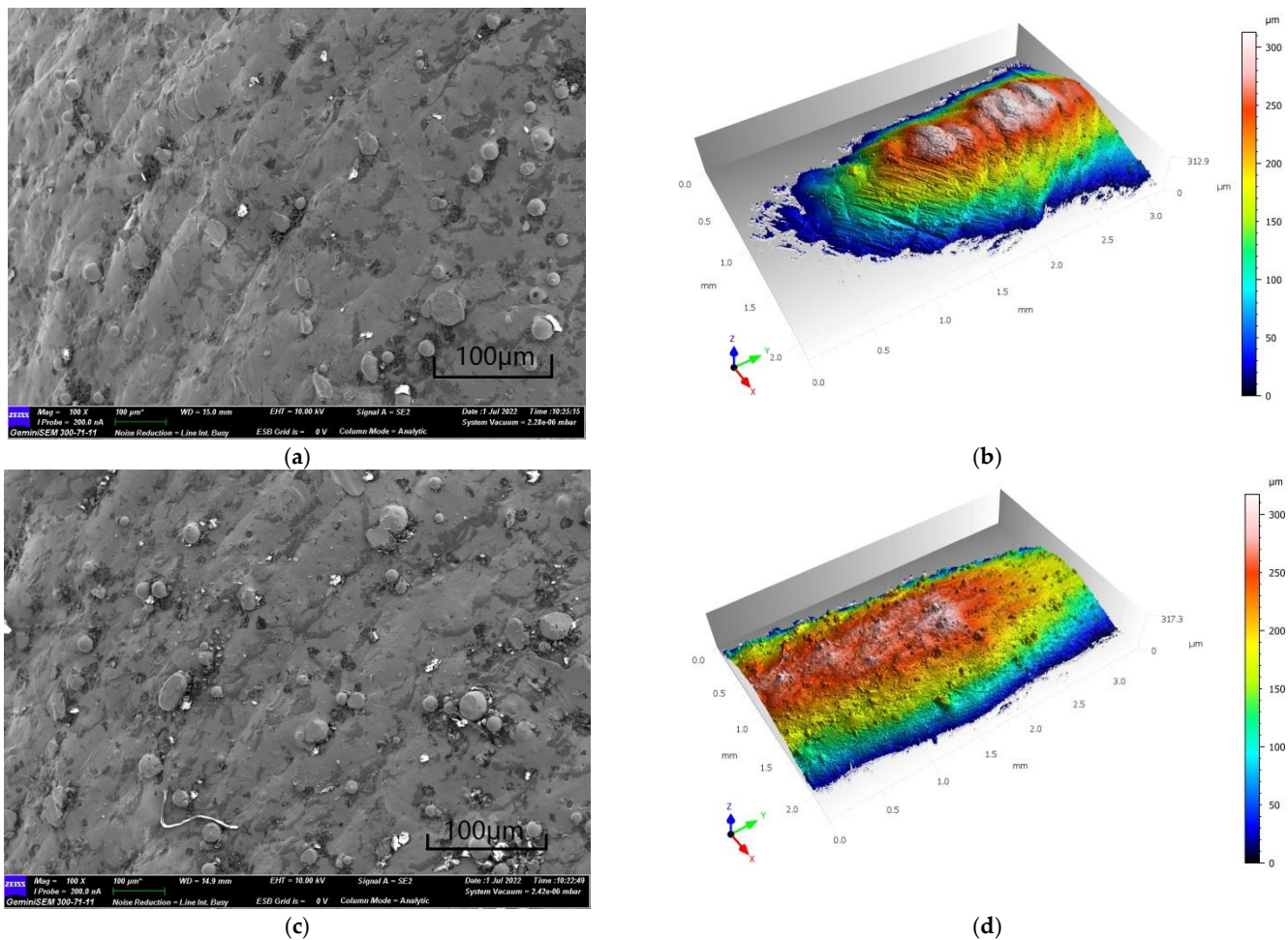


Figure 9. SEM images and 3D profiles of Part C': (a,b) horizontal plane; (c,d) vertical surface.

4.2. Optimized Parameters of Dual-Beam Laser Polishing

In the parts created by laser metal additive manufacturing, the surface roughness is not always ideal. A surface roughness (S_a) of less than 5 µm for laser-selective melting martensitic aging die steel is currently considered to be relatively low level [17,46–48]. Both of the laser beams that are used in these processes are flat-topped beams. The power of the infrared continuous laser is strong and it is mainly used for rough polishing. Additionally,

the power of the infrared pulse laser is weak and it is mainly used for sub-mirror or mirror polishing after rough polishing. In this process, firstly, the free-form surfaces of the high-strength parts formed by metal additive manufacturing are polished to a roughness of $R_a < 4 \mu\text{m}$ by an infrared continuous laser. The free-form surface is then polished to $R_a < 2 \mu\text{m}$ by an infrared pulse laser, to sub-specular or specular degree. Optimizing the laser polishing process parameters to ensure the peaks fill valley is difficult. The tension of the molten pool will be too large or too small, meaning that the peak cannot “just” fill the trough, and further reducing the surface roughness is difficult. When using Gaussian laser-beam polishing, the energy density in the center of the spot is too large, directly leading to metal gasification and leaving many pits on the polished surface. Using a flat-topped beam instead of a Gaussian beam ensures that the microscopic crest is only melted and avoids vaporization. Optimized parameters of dual-beam laser polishing are shown in Table 5.

Table 5. Optimized parameters of dual-beam laser polishing.

Factor Name	Optimized Value or Feature					
Roughness of initial state (nm)	6198	6365	6888	6922	7128	7920
Scanning speed (mm/s)	1000	900	850	800	750	650
CW power	200 W, 400 W, 600 W					
Pulsed laser (PW)	60 W					
Top-hat beam profile	Between medium and ideal					
Polishing parameters	Wavelength: 1080 nm; step-over: 0.1 mm					

The polished roughness value relative to the initial roughness value is shown in Figure 10. The graph shows the roughness of the double-laser-beam polished surfaces corresponding to each initial rough ground surface with a double-laser-beam polishing power varying from 200 W to 600 W by a single factor test method experiment. The surface roughness after polishing is not only related to the polishing process parameters, but also to the original roughness. Figure 10 shows that after a double-laser-beam polishing with the optimal parameters (CW 400 W + 60 W, $v = 800 \text{ mm/s}$), the surface roughness was significantly reduced to improve the service life of the high-strength MS metal materials from an initial roughness of $S_a = 6.198 \mu\text{m}$ to $S_a = 0.98 \mu\text{m}$ and from an initial roughness of $S_a = 7.92 \mu\text{m}$ to $S_a = 1.37 \mu\text{m}$, with a CW laser power of 400 W and a pulsed laser power of 60 W. Scale Point C's error bar with scale is shown in Figure 10, which reveals the difference in the roughness measured by polishing in different regions of three samples of high-intensity MS laser additive manufacturing.

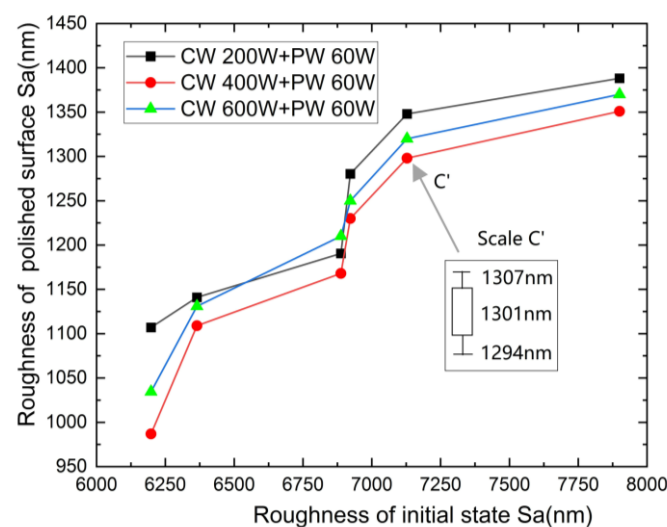


Figure 10. Polished roughness related to initial roughness.

Current studies focus on the horizontal and vertical building orientations considering different LPBF modes [49–52]. In LPBF, we distinguish the surfaces “horizontal” and “vertical” with respect to the building direction. Figures 11–13 shows that three samples formed LPBF after horizontal polishing. Figure 11a shows a flat polished sample, Figure 11b shows a freeform surface of a high-strength metal additive formed in Part B’, and Figure 11c shows a freeform surface of a high-strength metal additive formed in Part C’. We used a continuous laser and a pulsed laser for multi-step polishing, which remarkably reduced the surface roughness. Additionally, the surface morphology was tested with confocal microscopy.

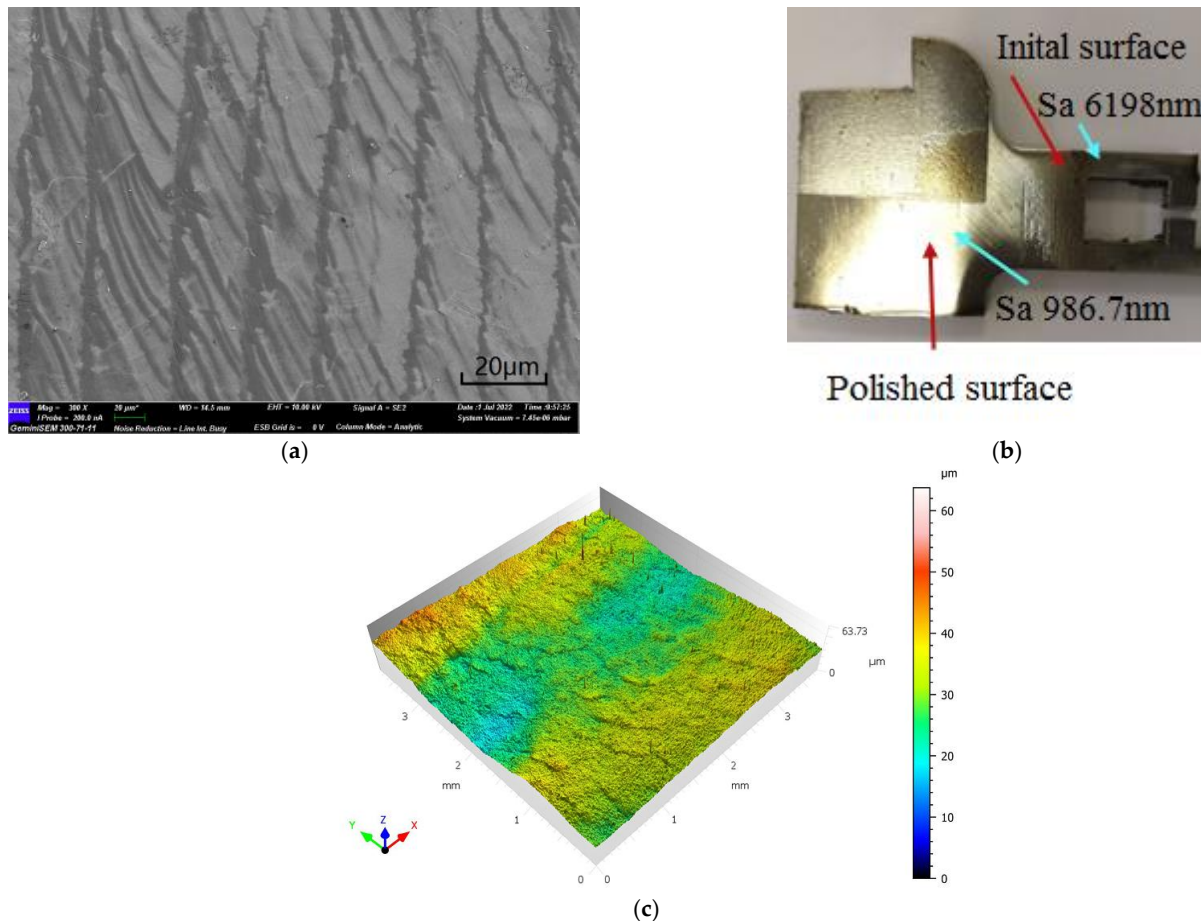


Figure 11. Polished specimen A’ and surface morphology of area A’. (a) SEM images of Part A’; (b) Polished specimen A’; (c) 3D profiles of A’.

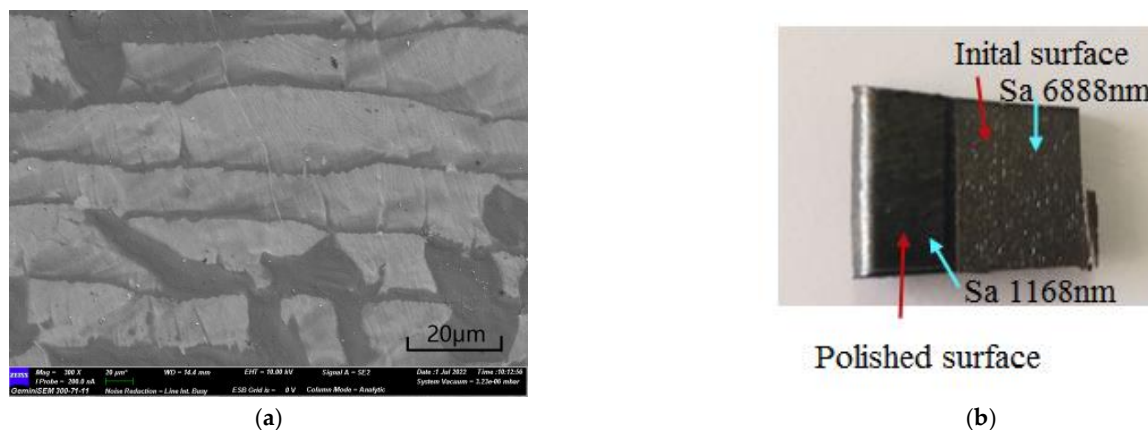


Figure 12. Cont.

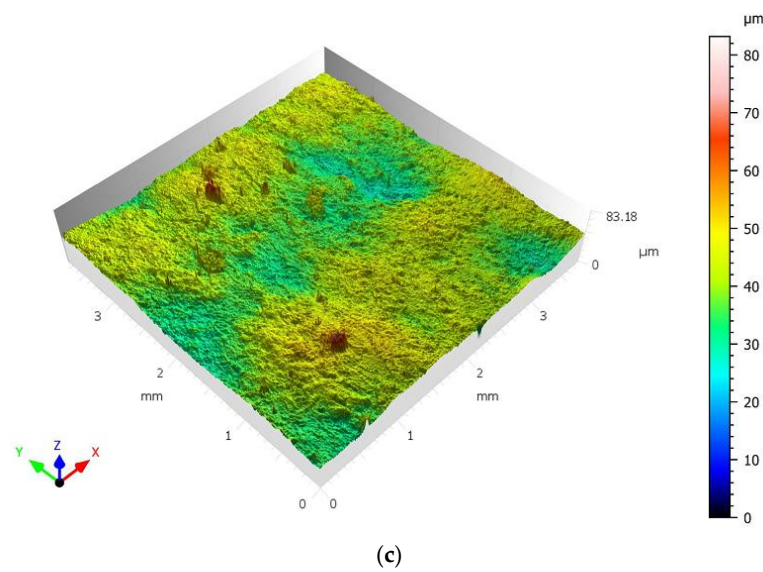
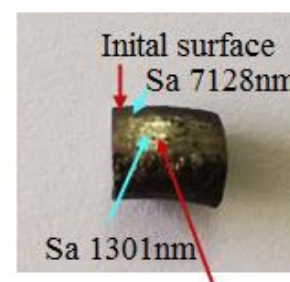
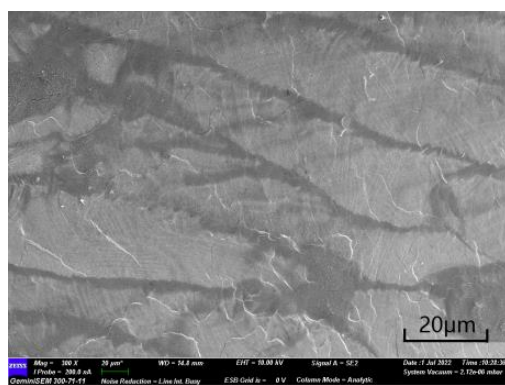


Figure 12. Polished specimen B' and surface morphology of area B'. (a) SEM images of Part B'; (b) Polished specimen B'; (c) 3D profiles of B'.



Polished surface

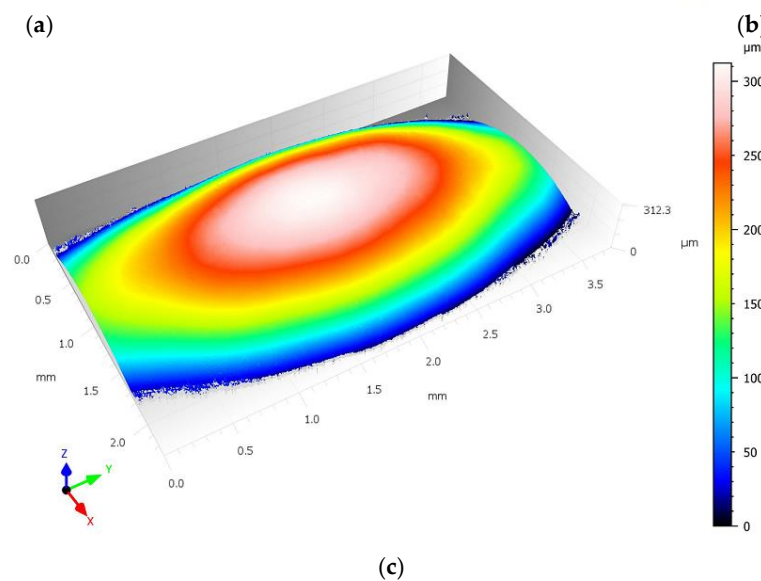


Figure 13. Polished specimen C' and surface morphology of area C'. (a) SEM images of Part C'; (b) Polished specimen C'; (c) 3D profiles of C'.

The lateral upper surface hardness value was higher than the original hardness value, indicating that the influence range on the surface roughness after polishing with a double laser beam was 1–2 mm; thus, the longitudinal surface hardness value was smaller. After double-laser-beam polishing metal additive manufacturing, the grain size of the material subject decreased and the lattice arrangement became neater. The surface structure of the MS metal additive steel was strengthened and improved by double-laser-beam polishing. The surface roughness in the transverse direction was obviously higher than the original hardness, indicating that the surface hardness of the laser-polished high-strength maraging steel metal material increased. The influence of the surface roughness in the longitudinal direction was 5 mm, indicating that the mechanical properties of the MS steel polished with a double laser beam had little influence in the longitudinal direction.

In the laser additive manufacturing process, the surface morphology of the parts is restricted by the process parameters used, creating unique morphology characteristics. The cross-section of the LPBF outer surface is similar to those reported in the literature [53]. The hardness test results and a comparison of laser-polished MS additive parts are shown in Figure 14. Figure 14a shows a diagram of a polishing hardness test and Figure 14b shows the hardness of the as-fabricated and MS products polished by LPBF. The hardness in the horizontal direction was slightly higher than that in the vertical direction, at about 35 HRC. The horizontal cross-section hardness after polishing was much harder than the original surface, whereas the vertical cross-section hardness, with a decreased maximal surface hardness and high residual tensile stresses from 34 HRC up to about 53 HRC, can be introduced with double-laser-beam polishing. Additionally, measurement errors are noted in Figure 14b.

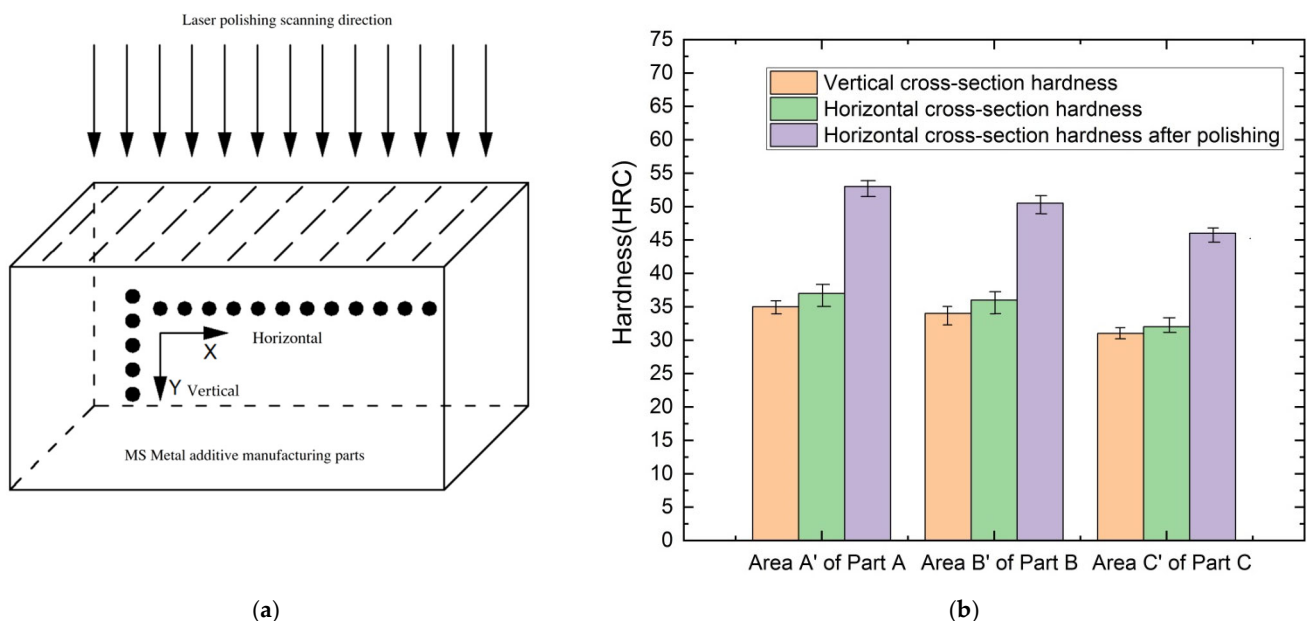


Figure 14. Hardness test and comparison of laser-polished MS additive parts. (a) diagram of polishing hardness test; (b) hardness of the as-fabricated and polished MS parts.

SEM images of the original formed surface and the polished layer are shown in Figure 15. Figure 15a shows the original formed surface and the polished layer. On higher magnification, the original formed surface of LPBF reveals distinctive segregation patterns in Figure 15b,c, which shows the melt zone and the heat-affected zone, the area where the microstructure and properties of the polishing layer change significantly during laser polishing. The austenite grains grow, from martensite to austenite during this peak temperature. In the top region of the polished layer, the grain size further decreases for the high cooling rate, as shown in Figure 15d on higher magnification, which shows the polished layer grain transformation. After the double-laser-beam polishing process,

different grain refinement structures and a re-oriented texture are presented. In addition, it also led to a considerable change in microhardness, for the transformation of martensite to austenite, grain size, morphology, and composition.

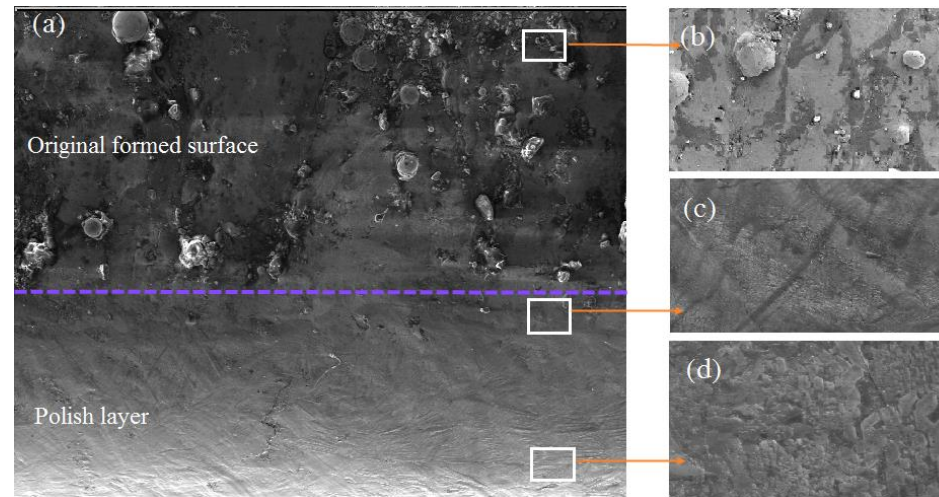


Figure 15. SEM images of the original formed surface and the polished layer. (a) Total of the original formed surface and the polished layer, (b) original formed surface, (c) melt zone and heat-affected zone, and (d) polished layer crystal.

Previous works adopt an effective XRD detection method and have demonstrated the reason for the grain transformation on the polished layer caused by the formation of the martensitic phase after rapid melting and cooling during laser polishing [32,54]. The polished layer of the MS parts was characterized using quantitative XRD analysis with HighScore plus 3.0 software (Xpert Highscore 3.0, Philips Analytical Instruments, Almelo city, Netherlands). Figure 16 shows the grain content of the XRD peak area. The original LPBF MS parts mainly consisted of martensite (α) and a small amount of austenite (γ) phases. Figure 16 shows that the XRD patterns obtained by the diffractometer were characterized by narrow “spikes” that were generally independent of each other. Before polishing, the XRD test result in the horizontal direction of the sample is similar to that in the longitudinal direction. After polishing, the XRD test results of the horizontal direction of the sample showed notable changes. The peak narrowness (γ 111 and γ 200) relatively increased after polishing, while at the same time, the content of martensite (α 110) decreased. In the same substance, this means that the crystallization was stronger. After polishing, the martensite content in the horizontal plane decreased from 97.5% to 90.2%. The X-ray diffraction (XRD) analysis results obtained for the samples before and after polishing are shown in Figure 16. Compared with the initial surface, the peak value of the martensite on the laser-polished surface decreased, but the peak value of the austenite phase increased, indicating that the microstructure of the laser-polished layer changed with the occurrence of grain refinement during the rapid melting process of the workpiece surface, and that the microstructure was different from that of the matrix.

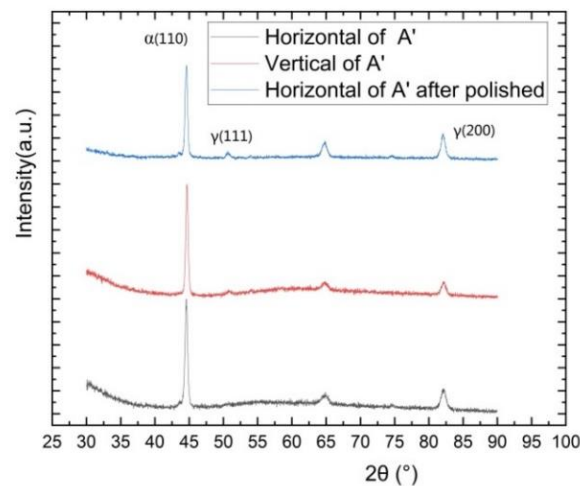


Figure 16. XRD analysis of the as-fabricated and polished MS specimens.

5. Conclusions

In summary, the properties of the maraging steel metal materials before and after LPBF polishing were compared and analyzed. A continuous laser and a pulsed laser were used to polish the surface with double laser beams, which remarkably reduced the surface roughness. LPBF polishing roughness reduction is an important factor affecting the LPBF component performance. The polished layer was characterized by a surface roughness measurement instrument, XRD, SEM, and nano hardness tester. We studied the microstructure and mechanical properties of the surface that had undergone laser surface polishing for the metal additive manufacturing of high-strength maraging steel metal material. Compared with the initial surface, the peak value of martensite on the laser-polished surface decreased, but the peak value of the austenite phase increased, indicating that the microstructure of the laser-polished layers changes with the occurrence of grain refinement during the rapid melting of the workpiece surface, and that the microstructure was different from that of the matrix. After polishing, the martensite content in the horizontal plane decreased, with the differences in both processes influencing the composition, morphology, and content of the martensite and austenite. This study is a part of ongoing research for improving the surface quality of the high-strength maraging steel metal materials.

Author Contributions: Conceptualization, H.X. and W.Z.; methodology, Y.Z. and M.L.; investigation, C.D. and H.X.; writing—original draft preparation, H.X. and Y.C.; writing—review and editing, Y.Z., C.D. and W.Z.; supervision, M.L. and Y.Z. All authors have read and agreed to the published version of the manuscript.

Funding: This work was financially supported by the Science and Technology Project of Guangdong Province (grant no. 2021A0505030013), the Scientific Research Project of General Universities in Guangdong Province (grant nos. 2021KCXTD058, 2022ZDZX3073), the Shenzhen Science and Technology Plan (grant nos. JSGG20191230162001814, JSGG20210420091802007), and the School-Enterprise Collaborative Project of Shenzhen Institute of Information Technology (grant no. SZIIT2022KJ075).

Institutional Review Board Statement: Not applicable.

Informed Consent Statement: Not applicable.

Data Availability Statement: Data underlying the results presented in this paper are available upon request from the corresponding author.

Acknowledgments: We would like to acknowledge the contributions to the theory of metal additive manufacturing and double-laser-beam polishing described in this paper. We acknowledge Lijun Wang and Huayi Gong for their help with the supervision and investigation.

Conflicts of Interest: The authors declare no conflict of interest.

References

1. Frazier, W.E. Metal additive manufacturing: A review. *J. Mater. Eng. Perform.* **2014**, *23*, 1917–1928. [\[CrossRef\]](#)
2. Zhang, Y.; Wu, L.; Guo, X.; Kane, S.; Deng, Y.; Jung, Y.G.; Lee, J.H.; Zhang, J. Additive manufacturing of metallic materials: A review. *J. Mater. Eng. Perform.* **2018**, *27*, 1–13. [\[CrossRef\]](#)
3. Herzog, D.; Seyda, V.; Wycisk, E.; Emmelmann, C. Additive manufacturing of metals. *Acta Mater.* **2016**, *117*, 371–392. [\[CrossRef\]](#)
4. Blakey-Milner, B.; Gradl, P. Metal additive manufacturing in aerospace: A review. *Mater. Des.* **2021**, *209*, 110008. [\[CrossRef\]](#)
5. Li, M.; Du, W. Metal Binder Jetting Additive Manufacturing: A Literature Review. *J. Manuf. Sci. Eng. Trans. ASME* **2020**, *142*, 090801. [\[CrossRef\]](#)
6. Liu, S.Y.; Shin, Y.C. Additive manufacturing of Ti6Al4V alloy: A review. *Mater. Des.* **2019**, *164*, 107552. [\[CrossRef\]](#)
7. DebRoy, T.; Wei, H.L. Additive manufacturing of metallic components—Process, structure and properties. *Prog. Mater. Sci.* **2018**, *92*, 112–224. [\[CrossRef\]](#)
8. Sames, W.J.; List, F.A. The metallurgy and processing science of metal additive manufacturing. *Int. Mater. Rev.* **2016**, *61*, 315–360. [\[CrossRef\]](#)
9. Lewandowski, J.J.; Seifi, M. Metal Additive Manufacturing: A Review of Mechanical Properties. *Ann. Rev. Mater. Res.* **2016**, *46*, 151–186. [\[CrossRef\]](#)
10. Kok, Y.; Tan, X.P.; Wang, P.; Nai, M.L.S. Anisotropy and heterogeneity of microstructure and mechanical properties in metal additive manufacturing: A critical review. *Mater. Des.* **2018**, *139*, 565–586. [\[CrossRef\]](#)
11. Lee, J.; Park, H.J.; Chai, S.; Kim, G.R.; Yong, H.; Bae, S.J.; Kwon, D. Review on Quality Control Methods in Metal Additive Manufacturing. *Appl. Sci.* **2021**, *11*, 1966. [\[CrossRef\]](#)
12. Aboulkhair, N.T.; Simonelli, M.; Parry, L.; Ashcroft, I.; Tuck, C. 3D printing of Aluminium alloys: Additive Manufacturing of Aluminium alloys using selective laser melting. *Prog. Mater. Sci.* **2019**, *106*, 100578. [\[CrossRef\]](#)
13. Garcia-Blanco, M.B.; Diaz-Fuentes, M. Comparative study of different surface treatments applied to Ti6Al4V parts produced by Selective Laser Melting. *Trans. Inst. Metal Finish.* **2021**, *99*, 274–280. [\[CrossRef\]](#)
14. Demir, A.G.; Previtali, B. Additive manufacturing of cardiovascular CoCr stents by selective laser melting. *Mater. Des.* **2017**, *119*, 338–350. [\[CrossRef\]](#)
15. Sarkar, S.; Kumar, C.S.; Nath, A.K. Effects of different surface modifications on the fatigue life of selective laser melted 15–5 PH stainless steel. *Mater. Sci. Eng. A* **2019**, *762*, 138109. [\[CrossRef\]](#)
16. Guo, J.; Song, C.P.; Fu, Y.Z.; Au, K.H. Internal Surface Quality Enhancement of Selective Laser Melted Inconel 718 by Abrasive Flow Machining. *J. Manuf. Sci. E* **2020**, *142*, 101003. [\[CrossRef\]](#)
17. Bhaduri, D.; Penchev, P.; Batal, A.; Dimov, S.; Soo, S.L.; Sten, S.; Harrysson, U.; Zhang, Z.; Dong, H. Laser polishing of 3D printed mesoscale components. *Appl. Surf. Sci.* **2017**, *405*, 29–46. [\[CrossRef\]](#)
18. Zhang, D.Q. Investigation of Laser Polishing of Four Selective Laser Melting Alloy Samples. *Appl. Sci.* **2020**, *10*, 760. [\[CrossRef\]](#)
19. Strano, G.; Hao, L.; Everson, R.M.; Evans, K.E. Surface roughness analysis, modelling and prediction in selective laser melting. *J. Mater. Process. Technol.* **2013**, *213*, 589–597. [\[CrossRef\]](#)
20. Metelkova, J.; Vanmunster, L.; Haitjema, H.; Van Hooreweder, B. Texture of inclined up-facing surfaces in laser powder bed fusion of metals. *Addit. Manuf.* **2021**, *42*, 101970. [\[CrossRef\]](#)
21. Mooney, B.; Kourousis, K.I. A Review of Factors Affecting the Mechanical Properties of Maraging Steel 300 Fabricated via Laser Powder Bed Fusion. *Metals* **2020**, *10*, 1273. [\[CrossRef\]](#)
22. Wüst, P.; Edelmann, A.; Hellmann, R. Areal Surface Roughness Optimization of Maraging Steel Parts Produced by Hybrid Additive Manufacturing. *Materials* **2020**, *13*, 418. [\[CrossRef\]](#) [\[PubMed\]](#)
23. Huang, S.; Narayan, R.L.; Tan, J.H.K.; Sing, S.L.; Yeong, W.Y. Resolving the porosity-unmelted inclusion dilemma during in-situ alloying of Ti34Nb via Laser Powder Bed Fusion. *Acta Mater.* **2020**, *204*, 116522. [\[CrossRef\]](#)
24. Wen, Y.; Zhang, B.; Narayan, R.L.; Wang, P.; Song, X.; Zhao, H.; Ramamurthy, U.; Qu, X. Laser powder bed fusion of compositionally graded CoCrMo-Inconel 718. *Addit. Manuf.* **2021**, *40*, 101926. [\[CrossRef\]](#)
25. Mower, T.M.; Long, M.J. Mechanical behavior of additive manufactured, powder-bed laser-fused materials. *Mater. Sci. Eng. A* **2016**, *651*, 198–213. [\[CrossRef\]](#)
26. Rosa, B.; Mognol, P.; Hascoet, J.Y. Laser polishing of additive laser manufacturing surfaces. *J. Laser Appl.* **2015**, *27*, S29102. [\[CrossRef\]](#)
27. Marimuthu, S.; Triantaphyllou, A. Laser polishing of selective laser melted components. *Int. J. Mach. Tools Manuf.* **2015**, *95*, 97–104. [\[CrossRef\]](#)
28. Ma, C.P.; Guan, Y.C.; Zhou, W. Laser polishing of additive manufactured Ti alloys. *Opt. Lasers Eng.* **2017**, *93*, 171–177. [\[CrossRef\]](#)
29. Yung, K.C.; Xiao, T.Y.; Choy, H.S.; Wang, W.J.; Cai, Z.X. Laser polishing of additive manufactured CoCr alloy components with complex surface geometry. *J. Mater. Process. Tech.* **2018**, *262*, 53–64. [\[CrossRef\]](#)
30. Li, Y.H.; Wang, B.; Ma, C.P. Material Characterization, Thermal Analysis and Mechanical Performance of a Laser-Polished Ti Alloy Prepared by Selective Laser Melting. *Metals* **2019**, *9*, 112. [\[CrossRef\]](#)
31. Bhaduri, D.; Bhaduri, D. Pulsed laser polishing of selective laser melted aluminium alloy parts. *Appl. Surf. Sci.* **2021**, *558*, 149887. [\[CrossRef\]](#)
32. Parvez, M.M.; Patel, S.; Isanaka, S.P.; Liou, F. A Novel Laser-Aided Machining and Polishing Process for Additive Manufacturing Materials with Multiple Endmill Emulating Scan Patterns. *Appl. Sci. Basel* **2021**, *11*, 9428. [\[CrossRef\]](#)

33. Rosa, B.; Mognol, P.; Hascoet, J.Y. Modelling and optimization of laser polishing of additive laser manufacturing surfaces. *Rapid Prototyp. J.* **2016**, *22*, 956–964. [\[CrossRef\]](#)
34. Rosa, B.; Hascoët, J.Y.; Mognol, P. Laser polishing of additive laser manufacturing surfaces: Methodology for parameter setting determination. *Int. J. Manuf. Res.* **2020**, *15*, 181. [\[CrossRef\]](#)
35. Yao, Y.; Zhou, R.; Zhang, C.; Mei, T.; Wu, M. Surface polishing technology for additive manufacturing of complex metal components. *Acta Aeronaut. Astronaut. Sin.* **2022**, *43*, 525202.
36. Temmler, A.; Liu, D.; Preußner, J.; Oeser, S.; Luo, J.; Poprawe, R.; Schleifenbaum, J.H. Influence of laser polishing on surface roughness and microstructural properties of the remelted surface boundary layer of tool steel H11—ScienceDirect. *Mater. Des.* **2020**, *192*, 108689. [\[CrossRef\]](#)
37. Braun, K.; Willenborg, E.; Schleifenbaum, J.H. Laser polishing as a new post process for 3D-printed polymer parts. *Procedia CIRP* **2020**, *94*, 134–138. [\[CrossRef\]](#)
38. Metelkova, J.; Vanmunster, L.; Haitjema, H.; Ordnung, D.; Kruth, J.P.; Van Hooreweder, B. Hybrid dual laser processing for improved quality of inclined up-facing surfaces in laser powder bed fusion of metals. *J. Mater. Process. Technol.* **2021**, *298*, 117263. [\[CrossRef\]](#)
39. Kumar, A.; Jayabalan, B.; Singh, C.; Jain, J.; Mukherjee, S.; Biswas, K.; Singh, S.S. Processing and properties of yttria and lanthana dispersed ODS duplex stainless steels. *Mater. Sci. Eng. A* **2022**, *837*, 142746. [\[CrossRef\]](#)
40. Kumar, P.; Zhu, Z.; Nai, S.M.; Narayan, R.L.; Ramamurty, U. Fracture toughness of 304L austenitic stainless steel produced by laser powder bed fusion. *Scr. Mater.* **2021**, *202*, 114002. [\[CrossRef\]](#)
41. Xiao, H.; Zhou, Y.; Liu, M.; Xu, X. Laser polishing of tool steel using a continuous-wave laser assisted by a steady magnetic field. *Aip Adv.* **2020**, *10*, 5116686. [\[CrossRef\]](#)
42. Sarafan, S.; Wanjara, P.; Gholipour, J.; Bernier, F.; Osman, M.; Sikan, F.; Molavi-Zarandi, M.; Soost, J.; Brochu, M. Evaluation of Maraging Steel Produced Using Hybrid Additive/Subtractive Manufacturing. *J. Manuf. Mater. Process.* **2021**, *5*, 107. [\[CrossRef\]](#)
43. Zhou, Y.Q.; Zhao, Z.Y.; Zhang, W.; Xiao, H.B.; Xu, X.M. Experiment Study of Rapid Laser Polishing of Freeform Steel Surface by Dual-Beam. *Coating* **2019**, *9*, 9050324. [\[CrossRef\]](#)
44. Bai, Y.; Yang, Y.; Wang, D.; Zhang, M. Influence mechanism of parameters process and mechanical properties evolution mechanism of maraging steel 300 by selective laser melting. *Mater. Sci. Eng. A* **2017**, *703*, 116–123. [\[CrossRef\]](#)
45. Chaolin, T.; Kesong, Z.; Wenyou, M.; Panpan, Z.; Min, L.; Tongchun, K. Microstructural evolution, nanoprecipitation behavior and mechanical properties of selective laser melted high-performance grade 300 maraging steel. *Mater. Des.* **2017**, *134*, 23–34.
46. Chaolin, T.; Kesong, Z.; Min, K.; Wenyou, M.; Tongchun, K. Microstructural characterization and properties of selective laser melted maraging steel with different build directions. *Sci. Technol. Adv. Mater.* **2018**, *19*, 746–758.
47. Cui, M.; Lu, L.; Zhang, Z.; Guan, Y. A Laser Scanner-Stage Synchronized System Supporting the Large-Area Precision Polishing of Additive-Manufactured Metallic Surfaces. *Engineering* **2021**, *7*, 1732–1740. [\[CrossRef\]](#)
48. Yung, K.C.; Zhang, S.S.; Duan, L.; Choy, H.S.; Cai, Z.X. Laser polishing of additive manufactured tool steel components using pulsed or continuous-wave lasers. *Int. J. Adv. Manuf. Technol.* **2019**, *105*, 425–440. [\[CrossRef\]](#)
49. Tridello, A.; Fiocchi, J.; Biffi, C.A.; Rossetto, M.; Tuissi, A.; Paolino, D.S. Size-effects affecting the fatigue response up to 10⁹ cycles (VHCF) of SLM AlSi10Mg specimens produced in horizontal and vertical directions. *Int. J. Fatigue* **2022**, *160*, 106825. [\[CrossRef\]](#)
50. Cai, W.; Song, Q.; Ji, H.; Gupta, M.K. Multi-Perspective Analysis of Building Orientation Effects on Microstructure, Mechanical and Surface Properties of SLM Ti6Al4V with Specific Geometry. *Materials* **2021**, *14*, 4392. [\[CrossRef\]](#)
51. Wu, S.Q.; Lu, Y.J.; Gan, Y.L.; Huang, T.T.; Zhao, C.Q.; Lin, J.J.; Guo, S.; Lin, J.X. Microstructural evolution and microhardness of a selective-laser-melted Ti-6Al-4V alloy after post heat treatments. *J. Alloy. Compd.* **2016**, *672*, 643–652. [\[CrossRef\]](#)
52. Kasperovich, G.; Becker, R.; Artzt, K.; Barriobero-Vila, P.; Requena, G.; Haubrich, J. The effect of build direction and geometric optimization in laser powder bed fusion of Inconel 718 structures with internal channels. *Mater. Des.* **2021**, *207*, 109858. [\[CrossRef\]](#)
53. Musekamp, J.; Hoche, H. Specific Characteristics of Materials Produced by Additive Manufacturing as Compared to Those Produced by Established Manufacturing Methods taking the Example of Alloy 718. *Prakt. Metallogr.* **2020**, *57*, 228–249. [\[CrossRef\]](#)
54. Zhihao, F.; Libin, L.; Longfei, C.; Yingchun, G. Laser polishing of additive manufactured superalloy. *Procedia CIRP* **2018**, *71*, 150–154. [\[CrossRef\]](#)